An effective strategy of constructing multi-junction structure by integrating heterojunction and homojunction to promote charge separation and transfer efficiency of WO_3

Yanting Li[1], Zhifeng Liu[1,2,3*], Junwei Li[1,2], Mengnan Ruan[1,2], Zhengang Guo[1,2]

(1 School of Materials Science and Engineering, Tianjin Chengjian University, 300384, Tianjin, China. 2 Tianjin Key Laboratory of Building Green Functional Materials, 300384, Tianjin, China. 3 Key Laboratory for Photonic and Electric Bandgap Materials, Ministry of Education, Harbin Normal University, Harbin, 150025, P. R. China.)

* corresponding author Tel: +86 22 23085236 E-mail: tjulzf@163.com

Supplemental Informations:

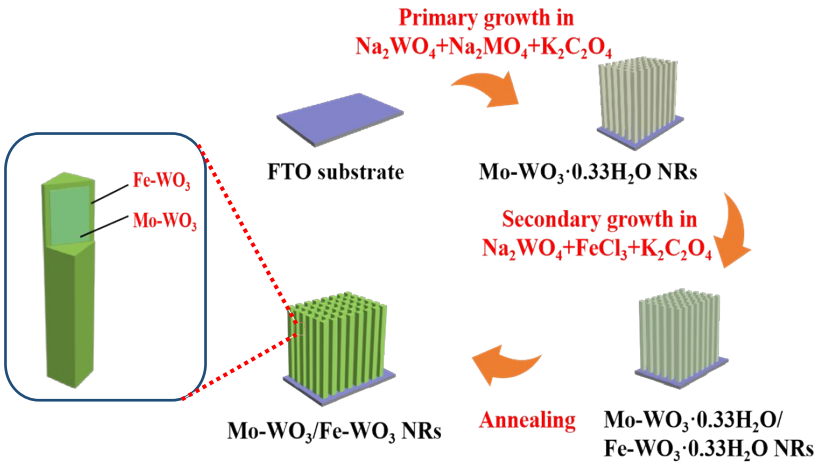

Fig. S1 Schematic illustration for the fabrication process of Mo-WO_3/Fe-WO_3 homojunction photoanode

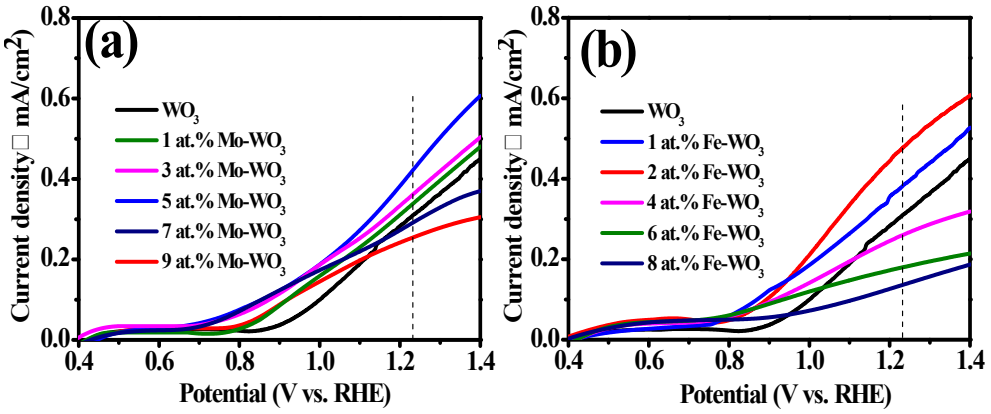

Fig. S2 LSV plots of WO_3 photoanodes with different Mo doping amounts (a) and with different Fe doping amounts (b) mearsured in 0.2 M Na_2SO_4 solution under AM 1.5 G illumination

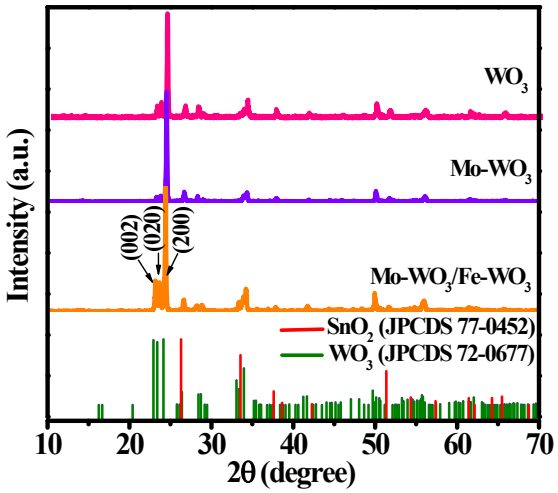

Fig. S3 XRD patterns of WO_3, Mo-WO_3 and Mo-WO_3/Fe-WO_3 homojunction Bottom peaks are standard positions of SnO_2 (red) and WO_3 (green)

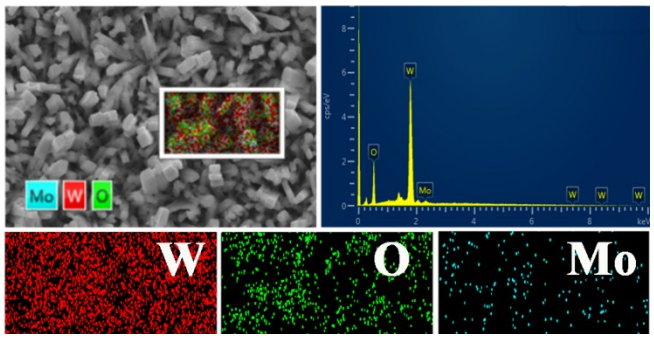

Fig.S4 EDS elemental analysis spectrum and corresponding elemental mapping images of W, O and Mo in Mo-WO_3, respectively

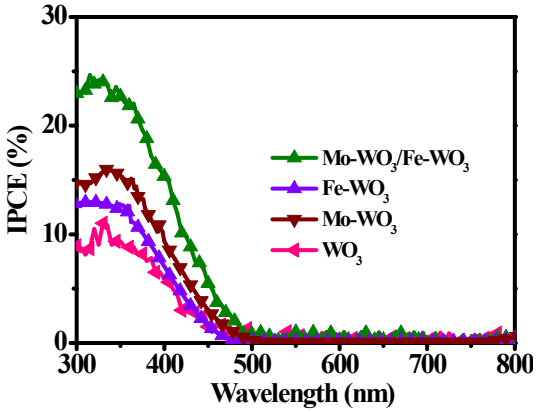

Fig.S5 Incident photon conversion efficiencies (IPCEs) plots of WO_3, Mo-WO_3/Fe-WO_3, Mo-WO_3/Bi_2S_3 and Mo-WO_3/Fe-WO_3/Bi_2S_3 photoanodes

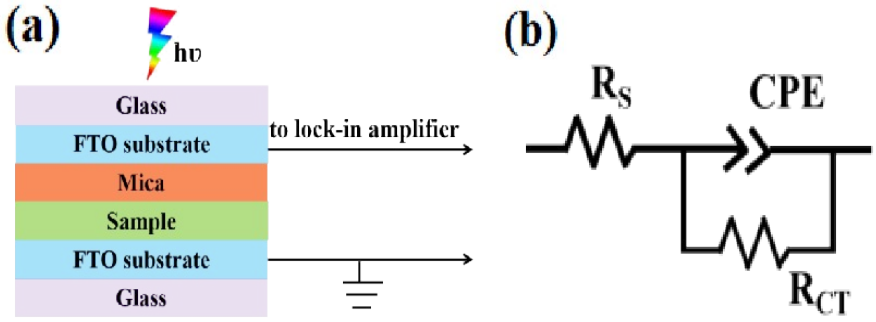

Fig. S6 (a) Schematic diagram of SPV measurement configuration. (b) The equivalent circuit of electrochemical impedance spectroscopy

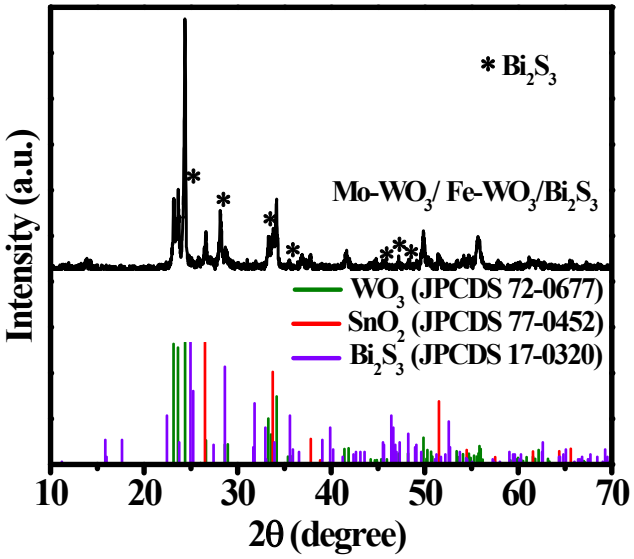

Fig. S7 XRD pattern of Mo-WO_3/Fe-WO_3/Bi_2S_3. Bottom peaks are standard positions of SnO_2, WO_3 and Bi_2S_3

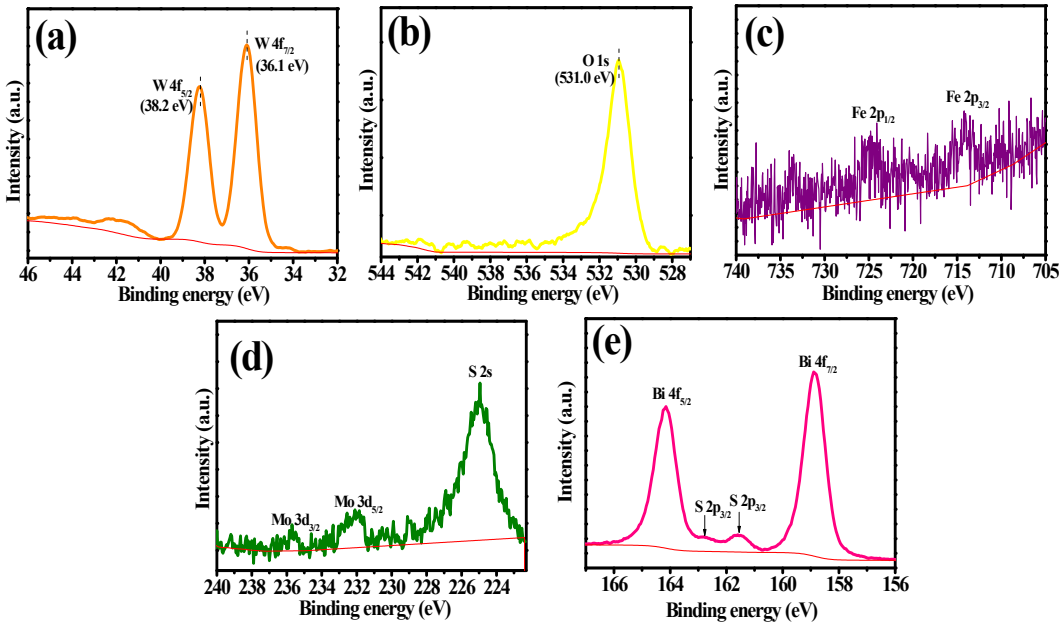

Fig. S8 High resolution XPS spectra of (a) W 4f, (b) O 1s, (c) Fe 2p, (d) Mo 3d and S 2s and (e) Bi 4f and S 2p for Mo-WO_3/Fe-WO_3/Bi_2S_3 composite

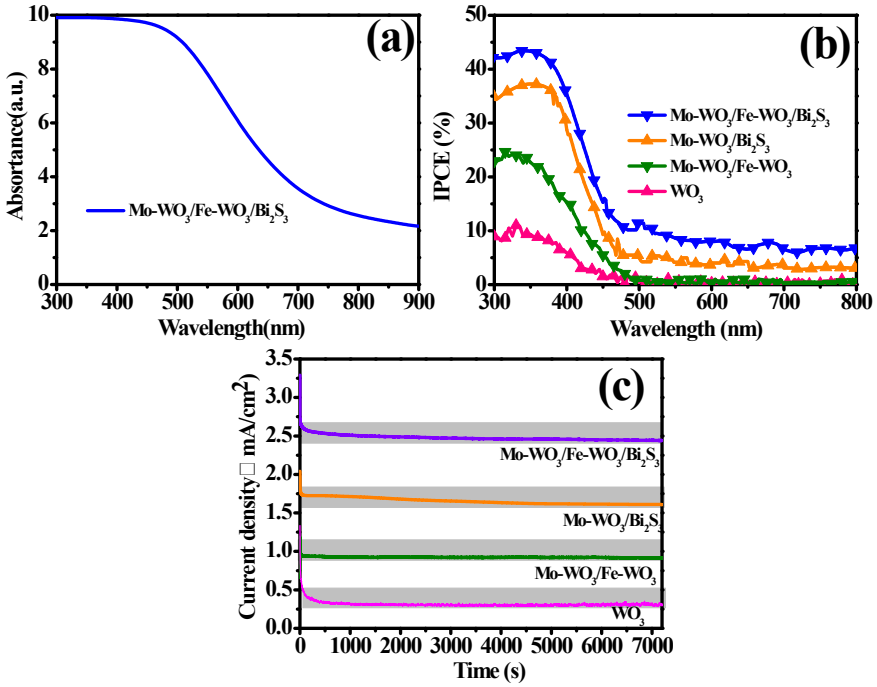

Fig. S9 (a) UV-Vis absorption spectrum of Mo-WO_3/Fe-WO_3/Bi_2S_3. (b) IPCEs plots. (c) Time-dependent photocurrent density curves of WO_3, Mo-WO_3/Fe-WO_3, Mo-WO_3/Bi_2S_3 and Mo-WO_3/Fe-WO_3/Bi_2S_3 photoanodes measured at 1.23V vs. RHE under simulated sunlight illumination for 7200 s

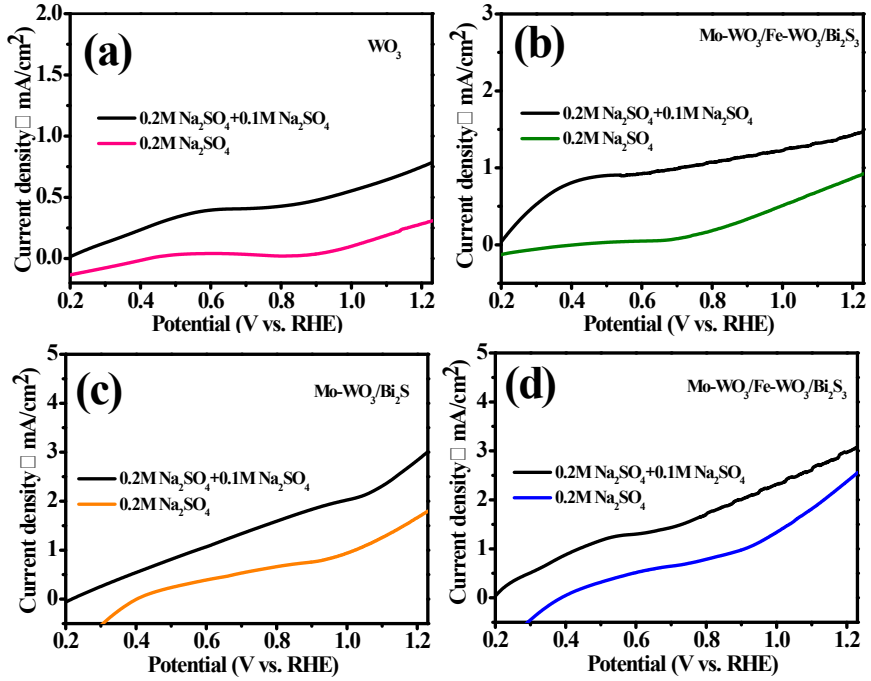

Fig. S10 LSV curves of WO_3, Mo-WO_3/Fe-WO_3, Mo-WO_3/Bi_2S_3 and Mo-WO_3/Fe-WO_3/Bi_2S_3 photoanodes measured in 0.2 M Na_2SO_4 electrolyte solution with the addition of 0.1 M Na_2SO_3

Tab. S1 The flat band potential (V_{FB}) and carrier density (N_d) of WO_3, Mo-WO_3, Fe-WO_3 and Mo-WO_3/Fe-WO_3 photoanodes

Sample	V_{FB} (V vs RHE)	N_d (cm^{-3})
WO_3	0.62	5.30×10^{19}
Mo-WO_3	0.56	1.19×10^{19}
Fe-WO_3	0.69	1.46×10^{19}
Mo-WO_3/Fe-WO_3	0.65	1.65×10^{20}

Tab. S2 EIS fitted parameters extracted from Nyquist plots of WO_3, Mo-WO_3, Fe-WO_3 and Mo-WO_3/Fe-WO_3 photoanodes

Sample	R_s (Ω cm^2)	R_{ct} (Ω cm^2)	CPE(F/cm^2)
WO_3	25	1752	2.10×10^{-3}
Mo-WO_3	28	1598	1.12×10^{-4}
Fe-WO_3	28	1407	2.67×10^{-4}
Mo-WO_3/Fe-WO_3	24	487	1.08×10^{-3}

Tab. S3 The flat band potential (V_{FB}) and carrier density (N_d) of Mo-WO_3/Bi_2S_3 and Mo-WO_3/Fe-WO_3/Bi_2S_3 photoanodes

Sample	V_{FB} (V vs RHE)	N_d (cm^{-3})
Mo-WO_3/Bi_2S_3	0.50	1.77×10^{22}
Mo-WO_3/Fe-WO_3/Bi_2S_3	0.59	3.62×10^{22}

Tab. S4 EIS fitted parameters extracted from Nyquist plots of Mo-WO_3/Bi_2S_3 and Mo-WO_3/Fe-WO_3/Bi_2S_3 photoanodes

Sample	R_s (Ω cm^2)	R_{ct} (Ω cm^2)	CPE(F/cm^2)
Mo-WO_3/Bi_2S_3	26	334	9.00×10^{-4}
Mo-WO_3/Fe-WO_3/Bi_2S_3	22	238	6.94×10^{-4}